Synthesis of nano$V_{3.6}Mo_{2.4}O_{16}$ and their catalytic activity in the selective oxidation of toluene

Ying Ying Liu[1], Huan Xia[2], Zhao Qing Liu[1], Zi Li Liu[1] ✉, Jian Liang Zuo[1]

[1]*Department of Chemical Engineering, Guangzhou University, Guangzhou 510006, People's Republic of China*
[2]*Department of Chemical Engineering, South China University of Technology University, Guangzhou 510006, People's Republic of China*
✉ *E-mail: gzdxlzl@gmail.com*

Published in Micro & Nano Letters; Received on 9th May 2018; Revised on 22nd July 2018; Accepted on 10th September 2018

Molybdenum vanadate is a novel vanadate. It is a functional material with good magnetic, electrical and catalytic properties. However, it is rarely used in the selective catalytic oxidation field, while the transition metal molybdenum and vanadium are usually used as a catalytic oxidation catalyst, the complex oxide and salt are naturally concerned. The structure of high-quality single crystalline Molybdenum vanadate ($V_{3.6}Mo_{2.4}O_{16}$) nanorods was synthesised by sol–gel method and high-temperature solid-state reaction. The effects of vanadium and molybdenum molar ratio and calcination temperature on the preparation of $V_{3.6}Mo_{2.4}O_{16}$ were studied. The structure of the catalyst was characterised by X-ray diffraction, thermogravimetry, X-ray photoelectron spectroscopy, scanning electron microscope and transmission electron microscope. The experimental results show that the molar ratio of vanadium–molybdenum is 10:7 when the precursor calcination temperature is 540°C, the single crystalline $V_{3.6}Mo_{2.4}O_{16}$ nanorods with regular shape has been obtained, the diameter of about 200 nm and the length up to tens of micrometres and the surface is smooth. Catalytic oxidation of toluene to benzaldehyde is used as a probe reaction for nano$V_{3.6}Mo_{2.4}O_{16}$. The catalytic activity of the catalyst is good, the conversion of toluene is 39.8% and the selectivity of benzaldehyde is 70.1%.

1. Introduction: Vanadate is an excellent functional material. It can be used as magnetic materials [1, 2], as cathode materials for lithium-ion batteries [3, 4]. It is widely used in the field of optical materials such as fluorescence and laser [5, 6]. However, it also has good catalytic properties, some of which have become mature industrial catalysts [7]. Their unique physical and chemical properties primarily come from the structure of the valence change of vanadium atoms and the interaction of their polyhedral structure of vanadium oxide, which can show many excellent properties [8, 9]. The nanostructures of metal vanadate can have different properties depending on their structure and composition. Different molybdenum vanadates have attracted wide attention due to its excellent catalytic, electrical and magnetic properties in the form of thin films, bulk powders and nanorods [10–13]. The complex nature makes them difficult to synthesise, especially their nanostructures. So far, there have been few reports on $V_{3.6}Mo_{2.4}O_{16}$ nanostructures. Therefore, it is very important to develop a simple and effective method for preparing nanoscale $V_{3.6}Mo_{2.4}O_{16}$. Here, we synthesised the nanostructured $V_{3.6}Mo_{2.4}O_{16}$ by sol–gel-high-temperature solid-state reaction.

The selective functionalisation of aromatic hydrocarbons is an important task in the industry; however, the cracking and oxidation of C–H bonds require high temperature, high pressure and efficiency catalysts, which are still a significant challenge [14, 15]. Toluene is an aromatic compound that can be oxidised to benzyl alcohol, benzaldehyde and benzyl benzoate [16]. Among them, benzaldehyde is the simplest and most important product; it is widely used in food, pharmaceutical, perfume and pesticide industries [17]. However, benzaldehyde is easily oxidised to benzoic acid. The traditional production route of benzaldehyde is the toluene chlorination and hydrolysis method. However, chlorine ion is inevitably left in the process, which is not easy to remove and produce a large amount of wastewater, resulting in environmental pollution and equipment corrosion [18–20]. What even worst is that benzaldehyde generated by this route cannot be used to synthesise certain high-quality compounds such as drugs or fragrances [21]. Therefore, it is very important to find a green benzaldehyde synthesis route and to develop an efficient catalyst for highly selective oxidation of toluene to benzaldehyde.

Xia *et al.* [22] used hydrogen peroxide (H_2O_2) as oxidant, the conversion of toluene on the V–Mo–Fe–O catalyst was 40.3% and the yield of benzaldehyde was 84.5%. Mo *et al.* [23] synthesised Silver vanadate ($Ag_2V_4O_{11}$) nanoribbons using the ultrasonic-hydrothermal method. The conversion of toluene on this ribbon-shaped nanocomposite catalyst was 42.5% and the selectivity to benzaldehyde was 56.4%. Here, we synthesised nanorod structure $V_{3.6}Mo_{2.4}O_{16}$ by sol–gel and high-temperature solid-phase reaction method, and catalytic oxidation toluene to benzaldehyde under mild conditions.

2. Experimental results: All the chemical reagents used in the experiments were obtained from commercial sources as guaranteed-grade reagents and used without further purification.

2.1. Catalyst preparation: In this experiment, citric acid was used as the complexing agent, synthesised the molybdenum vanadate catalyst by sol–gel and high-temperature solid-phase reaction. According to the design of the material ratio, weighed amount of Ammonium vanadate (NH_4VO_3) and Ammonium molybdate tetrahydrate ($(NH_4)_6Mo_7O_{24}4H_2O$), mixed in 20 ml of deionised water, stirred at 80°C for 30 min, then according to the molar ratio of *n*(Citrate Acid Anhydrous ($C_6H_8O7H_2O$)): *n* ($(NH_4)_6Mo_7O_{24}4H_2O$) = 8:1, slowly added citric acid, stirred for 1 h to form a sol, and then the mixed sol was heated up to 100°C and stirred for 2 h to form a gel. The gel was dried at 80°C under vacuum for 10 h, and finally calcined at a certain temperature to obtain a catalyst sample.

2.2. Catalytic performance evaluation tests: Liquid phase oxidation of toluene was carried out in a three-neck round-bottom flask, and 0.2 g $V_{3.6}Mo_{2.4}O_{16}$ catalysts, 2 ml toluene, and 15 ml acetic acid used as a solvent, were added, and 30 wt% H_2O_2 was subsequently added dropwise and reacted at 80°C for 30 min. After the reaction,

doi: 10.1049/mnl.2018.5151

the solid catalysts were separated by filtration, and the products were analysed by using a gas chromatograph (Shimadzu, GC-2014) equipped with an HP5 capillary column and a flame ionisation detector and using the peak-area internal standard method.

2.3. Characterisations: The crystal structure of the catalyst was analysed by a MASAL XD-3 diffractometer (Beijing Purkinje company). The test conditions were as follows: copper Kα ray ($\lambda = 0.15406$ nm), tube voltage and tube current were 36 kV, 20 mA, respectively. Scanning speed of 8°/min. X-ray photoelectron spectroscopy (XPS) was performed using a multi-functional X-ray photoelectron spectrometer (Shimadzu Axis Ultra DLD, Kratos, UK). Analytical catalyst synthesis thermal analysis using SDT Q600 integrated thermal analyser (US TA company) and differential scanning calorimeter differential scanning calorimetry (DSC) 204 F1 (Germany Chi equipment company), test conditions: carrier gas is air, the flow rate is 100 ml/min, increase from 30 to 650°C at 10°C/min. The sample was scanned using the Japanese Electron Plant Model JSM-7001F thermal field-emission scanning electron microscope (SEM). The working voltage was 10 kV. Before the test, the sample was pre-vacuum-sprayed to increase its conductivity. Transmission electron microscope (TEM) was measured at 200 kV on a field-emission TEM Tecnai G2 F20 S-TWIN (FEI USA).

3. Results and discussion

3.1. Comprehensive thermal analysis of catalyst precursors: The catalyst was calcined at high-temperature through a certain ratio of the mixed vanadium–molybdenum precursor, so the roasting process is very important for the formation of the catalyst. The catalyst precursor was prepared by the sol–gel method of ammonium molybdate and ammonium metavanadate (vanadium–molybdenum molar ratio of 10: 7), and the thermal analysis of the catalyst precursor was carried out by thermogravimetry (TG) and DSC. The thermochemical process of catalyst synthesis is investigated and the results are shown in Fig. 1.

From Fig. 1, the catalyst precursor has a fast weightlessness peak at 100 and 250°C. At the same time, the corresponding endothermic peak appears on the DSC chart, corresponding to the thermal dehydration of the catalyst precursors and the decomposition of ammonium salts. At 440−530°C, there is a relatively large weightlessness peak. At the same time, DSC shows the corresponding exothermic peak, indicating that the catalyst precursor decomposes and forms molybdenum vanadate in this temperature region. The molybdenum vanadate begins to form at 440°C. When the temperature is above 530°C, the weight will no longer change. However, the DSC chart shows continue to exotherm, indicating that the catalyst undergoes solid-phase reaction and crystal transition at 530°C. It can also be seen from the SEM photograph of Fig. 2 that the precursor forms a uniform rod-like crystal structure through high temperature.

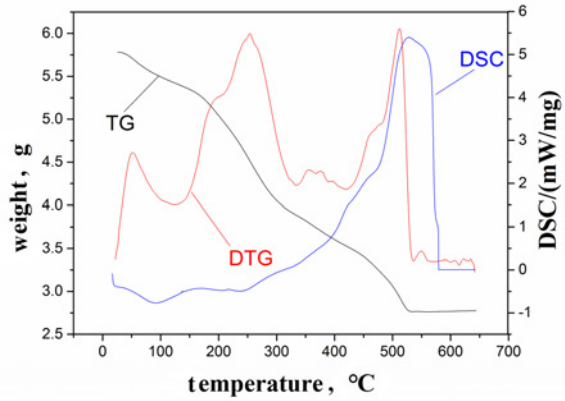

Fig. 1 *Thermograms of vanadium–molybdenum compound precursor*

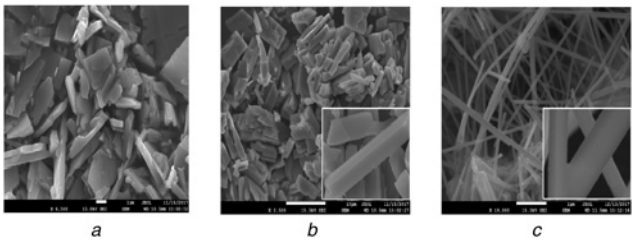

Fig. 2 *SEM images of the catalyst sample*
a Calcination for 3 h at 440°C of V:Mo of 10:7
b Calcination for 3 h at 500°C of V:Mo of 10:7
c Calcination for 3 h at 540°C of V:Mo of 10:7

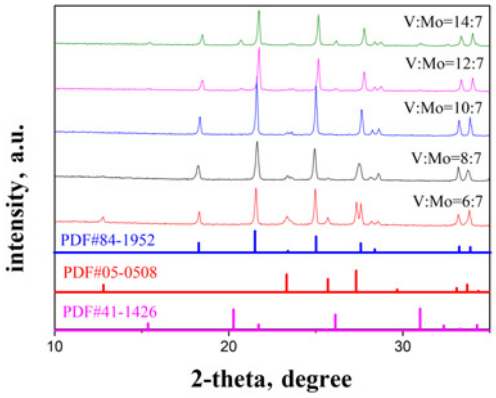

Fig. 3 *XRD patterns of the catalyst with various V:Mo mole ratio*

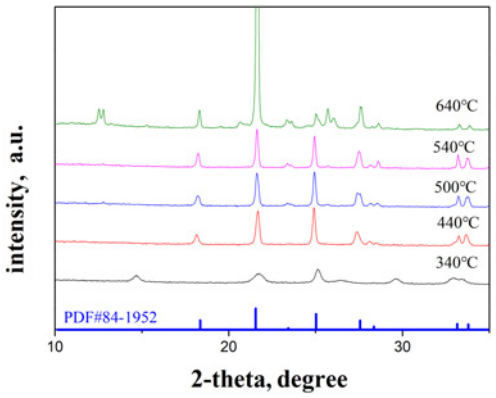

Fig. 4 *XRD patterns of catalyst samples with molar ratios of V:Mo of 10:7 at different calcination temperatures*

3.2. X-ray diffraction (XRD) analysis: The XRD patterns of catalysts were shown in Figs. 3 and 4.

From Fig. 3, we can see that with the increasing vanadium content, the diffraction peaks of Molybdenum trioxide (MoO_3) (JCPDF no. 05-0508) [24] at $2\theta = 13°$, 23°, 25.5°, 27°, 33.2° and 33.8° in the XRD pattern are constantly decreasing, and the diffraction peaks of molybdenum vanadate ($V_{3.6}Mo_{2.4}O_{16}$) at $2\theta = 18.5°$, 21.5°, 23.5°, 25°, 27.5°, 28.5° and 33.5°, 34° is constantly increasing. Through comparison and analysis, it was found that the molar ratio of vanadium–molybdenum increases from 6:7 to 10:7, the content of vanadium increased continuously, the diffraction peak of MoO_3 decreases. When the vanadium–molybdenum molar ratio was 10:7, MoO_3 diffraction peak almost disappeared, the pure $V_{3.6}Mo_{2.4}O_{16}$ phase (JCPDF no. 84-1952) was obtained. When the content of vanadium continues to increase, the molar ratio of vanadium to molybdenum increased from 10:7 to 14:7. The diffraction peaks of Vanadic anhydride (V_2O_5) (JCPDF no. 41-1426) [25] at $2\theta = 15.5°$, 20.5°, 26° and 31° appear in the XRD pattern.

When the ratio of vanadium to molybdenum is 10:7, the precursors are calcined at different temperatures. As can be seen from Fig. 4, the $V_{3.6}Mo_{2.4}O_{16}$ phase begins to form at 340°C. When the calcination temperature reaches 440°C, the diffraction peak of $V_{3.6}Mo_{2.4}O_{16}$ (JCPDF no. 84-1952) is basically complete. When the calcination temperature increased to 500 or 540°C, the peak intensity increased slightly and the pure $V_{3.6}Mo_{2.4}O_{16}$ phase was obtained. This result is consistent with the above thermal synthesis analysis. When the calcination temperature reaches 640°C, the diffraction peak changed greatly, the diffraction peak at $2\theta = 23.5°$ increased greatly, some other impurity peaks appeared, while the diffraction peaks of the other crystal planes of $V_{3.6}Mo_{2.4}O_{16}$ phase decreased. This may be due to the change in its crystal face caused by the temperature changes. It can be seen from the SEM image that 540°C is the optimum firing temperature.

3.3. XPS analysis: To further study the chemical composition and oxidation state of the obtained samples, XPS and atomic emission spectrometer analysis was performed on the catalyst.

As shown in Fig. 5*a*, the binding energy of O1s is 530.0 and 531.3 eV, corresponding to lattice oxygen and surface oxygen [26], respectively. Among them, lattice oxygen dominates, indicating that part of the catalyst surface has occurred hydroxylation reaction. Fig. 5*b* shows that the binding energy of Mo3d3/2 is 233.15 eV and the binding energy of Mo3d5/2 is 236.3 eV. The dual Mo(3d) lines are separated by 3.2 eV and the intensity ratio is 2:3. The Mo3d5/2 binding energies of Mo, Molybdenum dioxide (MoO_2) and MoO_3 were 228.0, 229.4 and 232.6 eV, respectively [13]. These results clearly provide evidence that the oxidation state of $V_{3.6}Mo_{2.4}O_{16}$ is + 6 (Mo^{6+}). Fig. 5*c* shows the XPS spectra of V 2p (V2p) spectrum, which shows two peaks binding energies of 524.8 and 517.5 eV, respectively, corresponding to V 2p1/2 and V 2p3/2 [27], shows that the valence of vanadium on the catalyst surface is V^{5+}.

3.4. SEM analysis: To understand the microstructure of the catalyst, the precursors with 10:7 ratio of vanadium to molybdenum were calcined at 440, 500 and 540°C for 1 h The SEM images are shown in Fig. 2.

From Fig. 2, the catalyst calcined at 440°C has an irregular bulk structure. The surface of the catalyst may be loaded by MoO_3. The catalyst calcined at 500°C begins to appear rod-like structure, and its surface is smooth, indicating that no MoO_3 existed. The results show that with the increase of temperature, the solid-state reaction takes place and the crystal form is transformed into rod-shaped $V_{3.6}Mo_{2.4}O_{16}$. However, the nanorods calcined at 500°C are irregular and have bulk structure. When calcined at 540°C, the nanorods with regular shape and uniform shape can be obtained. The diameter is about 200 nm and the length can reach dozens of microns. The surface is smooth and clean. It is shown that the crystal form is further changed with the increase in temperature. However, further increasing the calcination temperature will lead to catalyst sintering. 540°C is the best calcination temperature, which is consistent with TG-DSC, XRD analysis results.

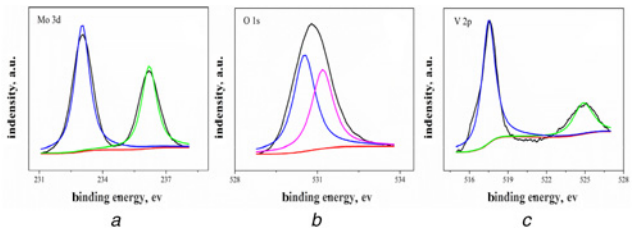

Fig. 5 *XPS of catalyst sample*
a XPS spectra of Mo 3d
b XPS spectra of O 1s
c XPS spectra of V 2p

3.5. TEM analysis: The microstructure of the prepared $V_{3.6}Mo_{2.4}O_{16}$ nanorods was further investigated by TEM measurement. The low-magnification TEM image shows the morphology of the nanorods (Fig. 6*a*), consistent with the above SEM observations. As shown in Fig. 6*c*, a single nanorod high-resolution TEM (HR-TEM) image, in which the lattice stripes are clearly visible. The distance between adjacent stripes is 0.41 nm, which is consistent with the (201) plane of the orthogonal $V_{3.6}Mo_{2.4}O_{16}$. Selected area electron diffraction (SAED) in Fig. 6*b* confirms the single crystal nature of nanorods. TEM analysis shows that the growth direction of the nanowires is in the ⟨001⟩ direction, resulting in an angle between the ribbon axis and the nanowire of 60°.

3.6. H_2-temperature program reduction (H_2-TPR) studies: Fig. 7 was the H_2-TPR profile of MoO_3, V_2O_5, and $V_{3.6}Mo_{2.4}O_{16}$.

From Fig. 7, in the $V_{3.6}Mo_{2.4}O_{16}$ catalyst, vanadium and molybdenum formed to pure $V_{3.6}Mo_{2.4}O_{16}$, which was confirmed by XRD and SEM. Hence, the H_2-TPR peaks of $V_{3.6}Mo_{2.4}O_{16}$ centred at 690°C attributed to the reduction of Mo^{6+}, and the peak centred at 550 and 580°C were the reduction of V^{5+}. In addition, the H_2-TPR peak of MoO_3 is 780°C, which is higher than the reduction peak of Mo^{6+} in $V_{3.6}Mo_{2.4}O_{16}$, and the H_2-TPR peaks of V_2O_5 are 670 and 710°C, which is also higher than the reduction peak of V^{5+} in $V_{3.6}Mo_{2.4}O_{16}$. The change of the reduction peak of $V_{3.6}Mo_{2.4}O_{16}$ catalyst shows that vanadium and molybdenum form $V_{3.6}Mo_{2.4}O_{16}$, accelerate the high-valence Mo to become low-valence Mo and high-valence V becomes low-valence V, and the lattice oxygen in the catalyst had a higher moving performance. Therefore, $V_{3.6}Mo_{2.4}O_{16}$ is more likely to promote oxidation of the active component and exhibit better catalytic oxidation activity.

3.7. Catalytic performance: The catalyst is used for selective catalytic oxidation of toluene. According to the literature [22], the optimum reaction conditions of toluene oxidation are as follows:

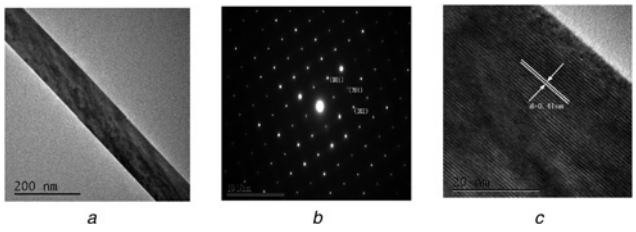

Fig. 6 *TEM images of catalyst sample*
a TEM images of catalyst sample
b SAED images of catalyst sample
c HR-TEM images of catalyst sample

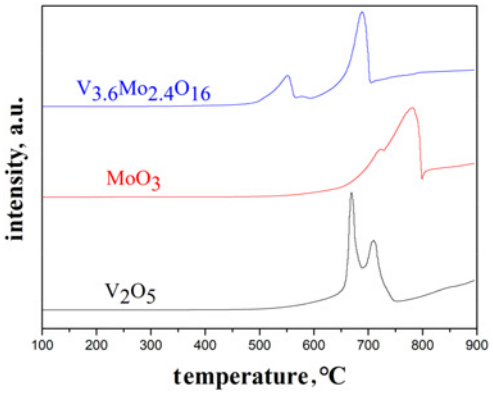

Fig. 7 *H_2-TPR profiles of MoO_3, V_2O_5 and $V_{3.6}Mo_{2.4}O_{16}$*

doi: 10.1049/mnl.2018.5151

Table 1 Effect of composition on the performance of catalysts

Catalysts	Toluene conversion, %	Benzaldehyde selectivity, %	Yield of benzaldehyde, %
MoO_3	3.2	72.5	2.3
V_2O_5	15.4	67.3	10.4
Fe_2O_3	3.4	37.7	1.3
$V_{3.6}Mo_{2.4}O_{16}$	39.8	70.1	27.9

Reaction conditions: catalyst 0.2 g, ice acetic acid as the solvent, H_2O_2 15 ml, $T = 80°C$, $t = 30$ min.

ice acetic acid as solvent, 15 ml of H_2O_2 and reaction at 80°C for 30 min. Toluene under this reaction conditions with different catalysts for oxidation. The influence of catalyst composition on the performance of the catalyst was investigated. The results are shown in Table 1.

From Table 1, when MoO_3 and V_2O_5 are used as catalysts only, the conversion of toluene is too low, but the selectivity to benzaldehyde is high. When Iron sesquioxide (Fe_2O_3) is used as a catalyst, the conversion and selectivity are too low. When $V_{3.6}Mo_{2.4}O_{16}$ synthesised by the sol–gel-high-temperature solid-state reaction method is used as a catalyst, the catalytic activity is very good. The conversion of toluene reached 39.8% and the benzaldehyde selectivity reached 70.1%.

The solvent has a great influence on the oxidation of toluene. Therefore, the effects of solvents with different acidity on the catalytic reaction were studied. The results are shown in Fig. 7.

From Fig. 8, when ice acetic acid is used as the solvent, both the-toluene conversion and benzaldehyde selectivity are the highest. The acidity of the solvent was found to be in the following order: ice acetic acid>acetonitrile>ethyl acetate. The conversion of toluene and the selectivity of benzaldehyde increased with increasing acidity of the solvent. It is indicated that the protons in the solvent may be involved in the catalytic reaction. The increase in acidity inhibits excessive oxidation, so selectivity increases, whereas the influence of the solvent acidity on catalytic reaction is complex. In addition, acetic acid has a proper polarity which can turn the reactants and H_2O_2 to form homogeneous reaction system favour the release of lattice oxygen of catalysts, it increased the toluene conversion.

SEM analysis showed that different calcination temperatures had a great influence on the morphology of the catalysts. Different temperatures will lead to different morphologies of the catalysts. Therefore, the effects of different calcination temperatures (different morphologies) on the catalytic performance were studied. The results are shown in Fig. 9.

From Fig. 9, the catalyst performance is poor when calcined at a low temperature, which may be due to the presence of MoO_3 and

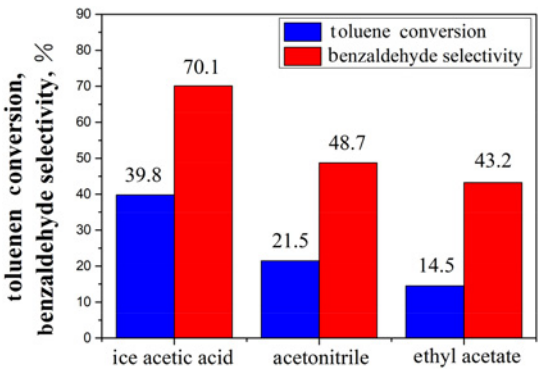

Fig. 8 *Effect of different solvents on the reaction performance reaction conditions: catalyst 0.2 g, ice acetic acid as the solvent, H_2O_2 15 ml, $T = 80°C$, $t = 30$ min*

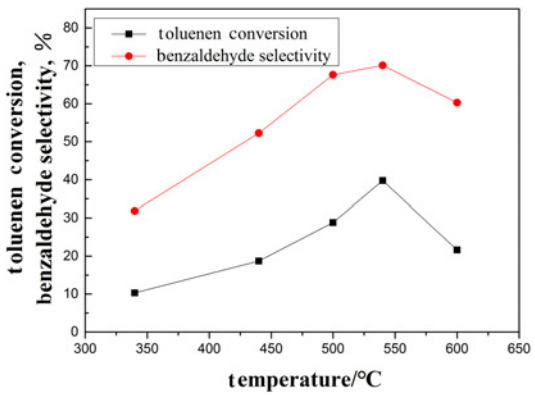

Fig. 9 *Effect of different calcination temperatures on the reaction performance reaction conditions: catalyst 0.2 g, ice acetic acid as the solvent, H_2O_2 15 ml, $T = 80°C$, $t = 30$ min*

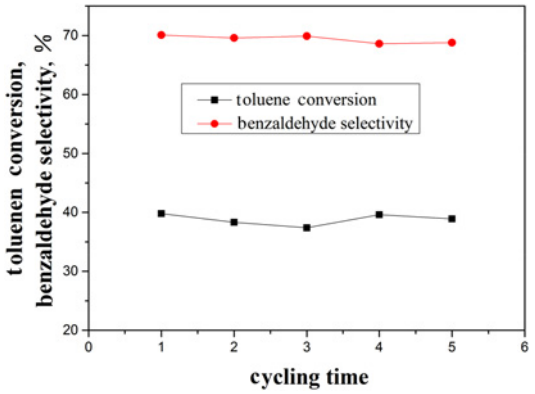

Fig. 10 *Effect of the number of catalyst cycles on the reaction performance reaction conditions: catalyst 0.2 g, ice acetic acid as the solvent, H_2O_2 15 ml, $T = 80°C$, $t = 30$ min*

V_2O_5 in the catalyst. With the increase of calcination temperature, pure $V_{3.6}Mo_{2.4}O_{16}$ gradually forms, its activity and selectivity increase. When the calcination temperature increased from 440 to 540°C, the morphology of the catalyst changed from bulk to regular-shaped nanorods. The catalytic activity increased from 18.7 to 39.8%, and the selectivity increased from 52.3 to 70.1%. As the calcination temperature increases further, the catalyst sintering together so that the rod structure cannot be maintained and the performance of the catalyst decreases. When the calcination temperature reaches 600°C, the activity decreases to 21.6% and the selectivity decreases to 60.3%. Therefore, the morphology of the catalyst has great influence on the catalytic performance, and the nanorod structure has the best catalytic performance.

Furthermore, in order to determine the reusability of the $V_{3.6}Mo_{2.4}O_{16}$ catalyst, reuse of the recovery catalyst had also been studied to further evaluate performance of the catalyst. After the first catalytic reaction, the solid was centrifugally separated from the reaction mixture, and then washed with acetone and dried. To obtain recovered catalyst was reused in the next five catalytic runs under the same reaction conditions, and the results are illustrated in Fig. 10. It was found that the $V_{3.6}Mo_{2.4}O_{16}$ catalyst could be reused at least five times. The reactivity of the reused catalyst slightly decreased, and the XRD patterns of the fresh and reused catalyst did not change, indicating that there was no obvious change of the surface and structure after the reaction and the quality of the reused catalyst did not change much, indicating no significant catalyst loss. This means that the catalyst can be efficiently recovered and reused.

4. Conclusions: The catalysts with different vanadium–molybdenum ratios were synthesised by sol–gel and high-temperature solid-state reaction method. When the vanadium–molybdenum ratio is 10:7, pure $V_{3.6}Mo_{2.4}O_{16}$ can be obtained. The results show that the ratio of vanadium to molybdenum has a significant effect on the formation of pure $V_{3.6}Mo_{2.4}O_{16}$, in addition, the calcination temperature has a great influence on the morphology of the catalyst. When the calcination temperature is 540°C and the ratio of vanadium–molybdenum is 10:7, the single crystalline $V_{3.6}Mo_{2.4}O_{16}$ nanorods with regular shape are obtained, the diameter of about 200 nm, the length up to tens of micrometres, the surface is smooth. The results of $V_{3.6}Mo_{2.4}O_{16}$ catalyst evaluation showed that the conversion of toluene reached 39.8% and the selectivity of benzaldehyde was 70.1%. Compared to other catalysts, the nanorod $V_{3.6}Mo_{2.4}O_{16}$ has high selectivity and high activity. In addition, the catalyst can be easily recycled and reused for five times without significant changes in its activity. It provides a new idea for the study of nanometre rod-shaped single crystal $V_{3.6}Mo_{2.4}O_{16}$ as a new type of vanadate used in the field of selective catalytic oxidation; it can be of wide application.

5. Acknowledgments: The authors gratefully acknowledge the financial support from the National Natural Science Foundation of China (grant no. 21676060) and the Major projects in Guangzhou (grant no. 201704020005).

6 References

[1] Marino N., Lloret F., Julve M., *ET AL.*: 'Synthetically persistent, self-assembled [V(IV)2V(V)4] polyoxovanadates: facile synthesis, structure and magnetic analysis', *Dalton Trans.*, 2011, **40**, (45), pp. 12248–12256

[2] Djerdj I., Cao M., Rocquefelte X., *ET AL.*: 'Structural characterization of a nanocrystalline inorganic–organic hybrid with fiber-like morphology and one-dimensional antiferromagnetic properties', *Chem. Mater.*, 2009, **21**, (14), pp. 3356–3369

[3] Koffer J.H., Olshansky J.H., Smith M.D., *ET AL.*: 'Formation principles for templated vanadium selenite oxalates', *Cryst. Growth Des.*, 2013, **13**, (10), pp. 4504–4511

[4] Pralong V., Caignaert V., Raveau B.: 'Transition metal hydrogenophosphates: a potential source of new protonic and lithium conductors', *J. Mater. Chem.*, 2011, **21**, (33), pp. 12188–12201

[5] Chen Z., Zhang Z., Dong X., *ET AL.*: 'Li_3VO_4: a promising mid-infrared nonlinear optical material with large laser damage threshold', *Cryst. Growth Des.*, 2017, **17**, (5), pp. 2792–2800

[6] Kong Q., Yang Y., Liu L., *ET AL.*: 'Density functional theory calculations, growth, structure, and optical properties of birefringent $LiNaV_2O_6$', *J. Mater. Res.*, 2016, **31**, (4), pp. 488–494

[7] Taufiq-Yap Y.H., Rownaghi A.A., Hussein M.Z., *ET AL.*: 'Preparation of vanadium phosphate catalysts from $VOPO_4{\cdot}2H_2O$: effect of microwave irradiation on morphology and catalytic property', *Catal. Lett.*, 2007, **119**, (1–2), pp. 64–71

[8] Zhang Z., Dong X., Chen Z., *ET AL.*: '$Pb_{10}V_6O_{25}$: a new lead vanadate with apatite structure', *J. Mol. Struct.*, 2018, **1151**, pp. 223–229

[9] Mi L., Huang Y., Qin C., *ET AL.*: 'Hydrothermal synthesis and optical properties of CsV_3O_8 microplates', *J. Lumin.*, 2018, **194**, pp. 414–419

[10] Duc F., Gonthier S., Brunelli M., *ET AL.*: 'Hydrothermal synthesis and structure determination of the new vanadium–molybdenum mixed oxide $V_{1.1}Mo_{0.9}O_5$ from synchrotron X-ray powder diffraction data', *J. Solid State Chem.*, 2006, **179**, (12), pp. 3591–3598

[11] Shahid M., Liu J., Ali Z., *ET AL.*: 'Structural and electrochemical properties of single crystalline MoV_2O_8, nanowires for energy storage devices', *J. Power Sources*, 2013, **230**, (10), pp. 277–281

[12] Yin Z., Xiao Y., Wang X., *ET AL.*: 'MoV_2O_8 nanostructures: controlled synthesis and lithium storage mechanism', *Nanoscale*, 2016, **8**, (1), p. 508

[13] Shakir I., Shahid M., Sarfraz M., *ET AL.*: 'Photocatalytic properties of single crystalline MoV_2O_8 nanowires', *Optoelectron. Adv. Mater.-Rapid Commun.*, 2014, **8**, (11), pp. 1068–1071

[14] Feng J.B., Wu X.F.: 'Oxidative synthesis of quinazolinones under metal-free conditions', *J. Heterocyclic Chem.*, 2017, **54**, (1), pp. 794–798

[15] Silva G.C., Carvalho N.M.F., Horn A.Jr., *ET AL.*: 'Oxidation of aromatic compounds by hydrogen peroxide catalyzed by mononuclear iron(III) complexes', *J. Mol. Catal. A, Chem.*, 2017, **426**, pp. 564–571

[16] Wang X., Wu G., Wang F., *ET AL.*: 'Solvent-free selective oxidation of toluene with O_2, catalysed by anion modified mesoporous mixed oxides with high thermal stability', *Catal. Commun.*, 2017, **98**, pp. 107–111

[17] Peedikakkal A.M.P., Jimoh A.A., Shaikh M.N., *ET AL.*: 'Mixed-metal metal–organic frameworks as catalysts for liquid-phase oxidation of toluene and cycloalkanes', *Arab. J. Sci. Eng.*, 2017, **42**, (10), pp. 4383–4390

[18] Jia L., Zhang S., Gu F., *ET AL.*: 'Highly selective gas-phase oxidation of benzyl alcohol to benzaldehyde over silver-containing hexagonal mesoporous silica', *Microporous Mesoporous Mater.*, 2012, **149**, (1), pp. 158–165

[19] Partenheimer W.: 'Methodology and scope of metal/bromide autoxidation of hydrocarbons', *Catal. Today*, 1995, **23**, (2), pp. 69–158

[20] Balaga V., Pedada J., Friedrich H.B., *ET AL.*: 'Tuning surface composition of Cs exchanged phosphomolybdic acid catalysts in CH bond activation of toluene to benzaldehyde at room temperature', *J. Mol. Catal. A, Chem.*, 2016, **425**, pp. 116–123

[21] Wang X., Wu G., Liu H., *ET AL.*: 'Solvent-free selective oxidation of toluene with O_2 catalyzed by metal cation modified LDHs and mixed oxides', *Catalysts*, 2016, **6**, (1), p. 14

[22] Xia H., Liu Z., Xu Y., *ET AL.*: 'Highly efficient V–Mo–Fe–O catalysts for selective oxidation of toluene to benzaldehyde', *Catal. Commun.*, 2016, **86**, pp. 72–76

[23] Mo M., Zheng M., Tang J., *ET AL.*: 'Selective oxidation of toluene using Ag nanoparticles self-supported on $Ag_2V_4O_{11}$ nanobelts', *Res. Chem. Intermed.*, 2013, **41**, (7), pp. 4067–4076

[24] Chen M., Ma X., Ma R., *ET AL.*: 'Ethanolysis of Kraft lignin over a reduction modified MoO_3 catalyst', *Ind. Eng. Chem. Res.*, 2017, **56**, (47), pp. 14025–14033

[25] Bhaskaruni S.V.H.S., Maddila S., van Zyl W.E., *ET AL.*: 'V_2O_5/ZrO_2 as an efficient reusable catalyst for the facile, green, one-pot synthesis of novel functionalized 1, 4-dihydropyridine derivatives', *Catal. Today*, 2018, **309**, pp. 276–281

[26] Dai Y., Wang X., Dai Q., *ET AL.*: 'Effect of Ce and La on the structure and activity of MnO_x catalyst in catalytic combustion of chlorobenzene', *Appl. Catal. B, Environ.*, 2012, **111**, pp. 141–149

[27] Yang G., Cui H., Yang G., *ET AL.*: 'Self-assembly of $Co_3V_2O_8$ multilayered nanosheets: controllable synthesis, excellent Li-storage properties, and investigation of electrochemical mechanism', *ACS Nano*, 2014, **8**, (5), pp. 4474–4487

doi: 10.1049/mnl.2018.5151